Crystal structure and domain-wall orientations of antiferroelectric $Pb(Yb_{1/2}Nb_{1/2})O_3$

1998 J. Phys.: Condens. Matter 10 5995

(http://iopscience.iop.org/0953-8984/10/26/023)

J. Phys.: Condens. Matter **10** (1998) 5995–6007. Printed in the UK PII: S0953-8984(98)92662-5

Crystal structure and domain-wall orientations of antiferroelectric $Pb(Yb_{1/2}Nb_{1/2})O_3$

Kyu Ho Park† and Woong Kil Choo

Department of Materials Science and Engineering, Korea Advanced Institute of Science and Technology, 373-1, Kusong-dong, Yusong-gu, Taejon 305-701, Korea

Received 17 March 1998

Abstract. The crystal structure of antiferroelectric $Pb(Yb_{1/2}Nb_{1/2})O_3$ with ordered complex perovskite structure was reexamined by TEM (transmission electron microscope). Its domain-wall orientations were investigated by the spontaneous strain method. From the CBED (convergent-beam electron diffraction) patterns, its point group was determined to be orthorhombic *mmm*. During transition from the high-temperature cubic to low-temperature orthorhombic phase, the prototype cubic cell is monoclinically distorted. The monoclinic cell was found to be contracted along the direction of Pb^{2+} shifts.

The reduced symmetry of the orthorhombic phase transformed from the prototypic phase allows the existence of ten species of domain walls, i.e. six W-walls and four W′-walls. The breaking of reflection symmetry during transition occurred at (1 0 0), (0 1 0), (0 1 1), (0 $\bar{1}$ 1), ($\bar{1}$ 0 1) and (1 0 1) planes of the cubic prototype. These high-symmetry planes correspond to the W-walls in the ferroelastic phase. Taking into account the domain geometry, the $(1\,0\,0)_m$ and $(0\,1\,0)_m$ planes are the 90° domain-boundaries and the others can be both 60° and 120° ones. The orientations of W′-walls calculated from the strain components were approximately $(\bar{2}\,3\,3)_m$, $(2\,\bar{3}\,3)_m$, $(\bar{3}\,2\,3)_m$ and $(3\,\bar{2}\,3)_m$ planes at room temperature. On approaching the transition these W′-walls tend to orient themselves toward the direction of 60° or 120° domain W-walls.

1. Introduction

Lead-based complex $Pb(B'_xB''_{1-x})O_3$ oxides of perovskite structure have attracted considerable attention for many years because of their interesting physical properties and wide industrial applications. Lead ytterbium niobate, $Pb(Yb_{1/2}Nb_{1/2})O_3$ (PYN), is an antiferroelectric exhibiting a sharp transition at 310 °C [1, 2] or 300 °C [3]. At high temperatures it possesses prototypic cubic ($m3m$) symmetry with the ordered cation (Yb^{3+}, Nb^{5+}) arrangements at the B-site [4]. The unit cell of high-temperature cubic phase is a doubled one ($2a_c \times 2a_c \times 2a_c$) in all the crystallographic axes of a cubic simple perovskite cell ($a_c \times a_c \times a_c$). The subscript c refers to the simple cubic perovskite unit cell, one eighth of the prototype supercell. When PYN is hypothetically assumed to be disordered, the unit cell size is simply $a_c \times a_c \times a_c$. The cation ordering is responsible for the cell doubling, which gives rise to the prototype supercell structure made of ten interpenetrating face centred cubic (fcc) sublattices. PYN undergoes a first-order structural phase transition from the paraelectric cubic to an antiferroelectric phase at the Curie temperature T_C.

The PYN crystal structure at room temperature was first proposed by Tomashpol'skii and Venevtsev [1], who showed by x-ray diffraction that Yb^{3+} and Nb^{5+} ions alternately

† E-mail address: khpark@cais.kaist.ac.kr

0953-8984/98/265995+13$19.50

occupied octahedral sites in the perovskite structure, and it was determined to be nearly monoclinic with lattice parameters $a_m = b_m = 4.168$ Å, $c_m = 4.107$ Å and $\gamma_m = 90°27'$. For this compound, in addition to the long range ordering of Yb^{3+} and Nb^{5+} ions at B-sites, antiparallel displacements of Pb^{2+} ions along the prototype $[1\,\bar{1}\,0]_c$ direction as in $PbZrO_3$ [5] were also confirmed by Kwon and Choo [4] from the superlattice reflections in x-ray and electron diffraction patterns. They revealed that the unit cell of antiferroelectric PYN is orthorhombic and that the orthorhombic unit cell has spacings $a_o = 5.918$ Å $\approx \sqrt{2}a'_c$, $b_o = 23.453$ Å $\approx 4\sqrt{2}a'_c$ and $c_o = 8.221$ Å $2a'_c$ at room temperature, where a'_c represents the lattice parameter of a simple pseudo-cubic perovskite unit cell of the prototype. The subscripts o hereafter denote the indices referred to the orthorhombic unit cell, while the subscript m refers to the monoclinic cell. Furthermore, the perovskite subcell at room temperature can be described as monoclinic because the lattice parameter a of a subcell is nearly equal to b and its lattice parameters were estimated to be $a_m = b_m = 4.168$ Å $\approx a'_c$, $c_m = 4.107$ Å $\approx a'_c$ and $\gamma_m = 89.47°$ at room temperature [6]. They also suggested that the space group of the orthorhombic phase is *Pbnm* if only the positions of the cations are taken into consideration and the lattice modulation due to Pb^{2+} displacements was given by the wave vectors $\{3/8\,3/8\,0\}_c$ while the B-site ordering wave was given by $\{1/2\,1/2\,1/2\}_c$. In reference to the prototype fcc superstructure, the former wave vectors may be equivalently written as $\{3/4\,3/4\,0\}_f$.

Below T_C, on the other hand, PYN is ferroelastic as well as antiferroelectric because it undergoes both the crystal system and point group symmetry changes during phase transition. On ferroelastic transition, the crystal of high-temperature phase also displays domains of different orientations. A theoretical approach to the ferroelastic domain structure can be effectively done by group analysis and spontaneous strain method. The group analysis provides the determination of permissible kinds of domain association and domain wall [7]. The lattice of a ferroelastic phase can be described as the prototype lattice spontaneously distorted under the action of spontaneous strains. Sapriel [8] derived the possible walls between adjacent domains in all the ferroelastic crystal systems from the criterion of spontaneous strain compatibility defined by Fousek and Janovec [9] for ferroelectric crystals. Both methods compare the characteristics of the high-temperature prototype phase and the low-symmetry one, and require the determination of the point groups of the two phases. The group analysis allows a very rapid determination of permissible walls, the orientation of which is attained by the spontaneous strain method. For PYN, the loss of most of symmetry elements of the cubic prototypic phase gives rise to a very complicated domain structure below T_C. Until now, no systematic investigation of domain-wall orientations of PYN has been conducted.

In spite of the previous reports, the exact crystal structure of antiferroelectric PYN has not been settled yet. In this paper, we would at least like to establish firmly the point group of the crystal PYN structure using transmission electron microscopy. Its point group is reexamined by convergent-beam electron diffraction studies. From the structural analysis, the evolution of domain-wall orientation changes of antiferroelectric PYN are also investigated on the basis of Sapriel's spontaneous strain method [8].

2. Experiment

Powders of PbO, Yb_2O_3 and Nb_2O_5 all having purity of 99.9 wt% were used as raw materials. The formation of perovskite phase has been shown to be enhanced by pre-reacting the B-site oxides first and by subsequent reaction with PbO [10]. A compound

of $YbNbO_4$ stochiometry was formed by calcination of Yb_2O_3 and Nb_2O_5 at 1100 °C for 4 h and then reacted with PbO to form stochiometric $Pb(Yb_{1/2}Nb_{1/2})O_3$ composition. The batch was calcined at 900 °C for 3 h to synthesize PYN. The ceramic bodies were then formed by sintering at 1120 °C for 2 h.

The powder specimens for x-ray investigation were prepared by grinding and seiving the calcined powders. X-ray measurements were performed on a two-circle Rigaku Rotaflex diffractometer using a high-temperature attachment. The diffractometer was scanned continuously in θ–2θ mode and the scanning speed of one degree (2θ) per 20 minutes was adopted. Specimens for electron-diffraction studies were prepared by mechanically polishing a bulk ceramic and thinning by argon-ion milling. The specimens were coated with carbon film a few tens of nm thick to stabilize them during observation. The TEM observations were done on a Phillips-CM20/T microscope operating at accelerating voltages of 200 and 120 kV, for a conventional TEM and CBED studies respectively.

3. Results and discussion

3.1. Crystal structure

Figure 1 shows a schematic projection of antiferroelectric (Pb^{2+}-displaced) PYN on $(001)_o$ as previously [4]. The prototype phase crystal class of PYN belongs to the point group $m3m$. Below T_C, this crystal is distorted to a monoclinic phase with $a_m \approx b_m$. The unit cell has orthorhombic symmetry. The orthorhombic lattice, compared to the monoclinic one, can be built on the vectors $\boldsymbol{a}_m$, $\boldsymbol{b}_m$ and $\boldsymbol{c}_m$ with:

$$\begin{aligned} \boldsymbol{a}_o &= \boldsymbol{a}_m + \boldsymbol{b}_m \\ \boldsymbol{b}_o &= 4(\boldsymbol{a}_m - \boldsymbol{b}_m) \\ \boldsymbol{c}_o &= 2\boldsymbol{c}_m. \end{aligned} \tag{1}$$

The orthorhombic parameters a_o, b_o and c_o are therefore:

$$\begin{aligned} a_o &= |\boldsymbol{a}_m + \boldsymbol{b}_m| = 2a_m \cos(\gamma_m/2) \\ b_o &= 4|\boldsymbol{a}_m - \boldsymbol{b}_m| = 8a_m \sin(\gamma_m/2) \\ c_o &= 2|\boldsymbol{c}_m|. \end{aligned} \tag{2}$$

At room temperature, the monoclinic parameters were found to be $a_m = b_m = 4.165$ Å, $c_m = 4.111$ Å and $\gamma_m = 89.47°$. The orthorhombic parameters were $a_o = 5.918$ Å, $b_o = 23.453$ Å and $c_o = 8.221$ Å. According to this scheme, a_o is slightly larger than $b_o/4$ (=5.863 Å). Consequently the perovskite cell of antiferroelectric PYN is extended along the polarization direction.

Figure 2 is an electron diffraction pattern taken in the $[0\,0\,1]_m$ (=$[0\,0\,2]_o$) zone at room temperature. The superlattices due to the antiparallel shifts of Pb^{2+} ions, as well as the fundamental spots of the prototype are shown in this pattern. It shows that the antiparallel Pb^{2+} displacements occur along the direction perpendicular to $\boldsymbol{R}_1$ with a wavevector (3/8 3/8 0). The strong superlattice spots correspond to the wavevector. Other weaker superlattice spots may be its higher order harmonics or may come from other source such as oxygen octahedral tilting. The monoclinic indexing of $\boldsymbol{R}_1$ for convenience' sake can be $(1\,1\,0)_m$ or $(1\,\bar{1}\,0)_m$ depending on Pb^{2+} displacements; Pb^{2+} ions move along the $[1\,\bar{1}\,0]_m$ or $[1\,1\,0]_m$ direction. We compared the two distances of $\boldsymbol{R}_1$ and $\boldsymbol{R}_2$ spots from the 000 spot, which are perpendicular and parallel to the direction of shifts of Pb^{2+} ions, respectively. In order to make an accurate measurement, higher order reflections of $\boldsymbol{R}_1$ and $\boldsymbol{R}_2$ were used.

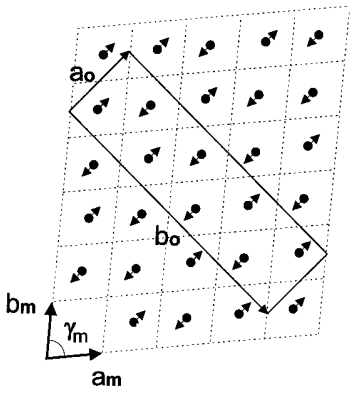

Figure 1. Antiferroelectric structure of $Pb(Yb_{1/2}Nb_{1/2})O_3$ on $(001)_o$ according to the model of Kwon and Choo [4]: the arrows represent the direction for Pb^{2+} ion shifts. Dashed lines delineate the perovskite cell and the solid line shows an orthorhombic unit cell. Other cation and anion positions are deleted for clarity.

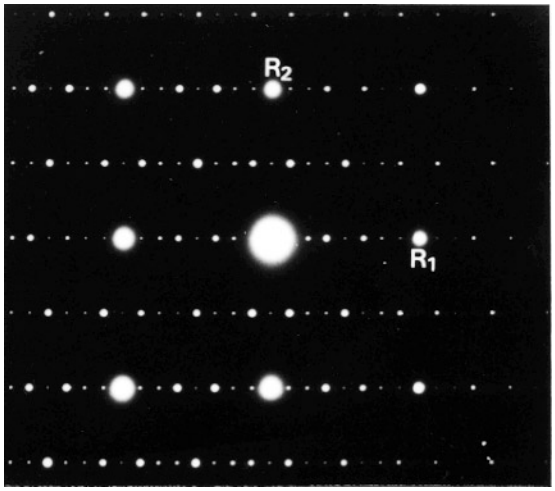

Figure 2. $[0\,0\,1]_m$ $(=[0\,0\,2]_o)$ zone-axis pattern from antiferroelectric $Pb(Yb_{1/2}Nb_{1/2})O_3$.

We found that the $|\boldsymbol{R}_2|/|\boldsymbol{R}_1|$ ratio was clearly larger than the unity, the value being 1.009. This indicates that the contraction of the orthorhombic cell occurs along the displacements of Pb^{2+} ions, although the value itself may not be accurate enough.

Among the several perovskite antiferroelectrics, the crystal structure of $PbZrO_3$ is most typical and best studied. Even for this compound, there have been also some unanswered questions in regard to the crystal structure. Shatalova *et al* [11] reported that the lattice slightly extends along the direction of Pb^{2+} shifts. But an amendatory interpretation for the monoclinic distortion of the perovskite cell was presented by Fujishita *et al* [12] and by Whatmore and Glazer [13] based upon x-ray profile analysis and the oscillation photographic method, respectively; the perovskite cell of antiferroelectric $PbZrO_3$ is contracted along the direction of shifts of Pb^{2+} ions. Since monoclinic PYN is much more distorted than monoclinic $PbZrO_3$ ($|\boldsymbol{R}_2|/|\boldsymbol{R}_1 = 1.0016$ by Fujishita *et al* [12]) at room temperature, the difference between two interplanar spacings could be compared with less ambiguity in the

electron diffraction pattern of PYN. Therefore the true orthorhombic unit cell of PYN, compared to the monoclinic lattice, can be represented by figure 3. According to this picture, the directions of Pb^{2+} shifts become $[1\,\bar{1}\,0]_m$ $(=[\bar{2}\,0\,0]_o)$ and $[\bar{1}\,1\,0]_m$ $(=[2\,0\,0]_o)$ and the monoclinic cell elongates along the $[1\,1\,0]_m$ $(=[0\,8\,0]_o)$ direction. Hereafter, all the indices of the planes and crystallographic axes of monoclinic and orthorhombic cells will be followed by the coordinate system already defined unless otherwise stated.

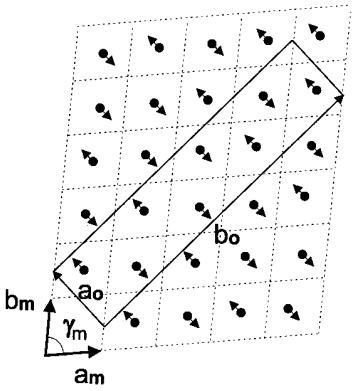

Figure 3. Schematic projection of antiferroelectric $Pb(Yb_{1/2}Nb_{1/2})O_3$ on $(001)_o$ explaining the amendatory interpretation for monoclinic distortion: the arrows represent the direction of Pb^{2+} ion shifts. Dashed lines mark the simple five-atom perovskite cell and the solid line shows the orthorhombic unit cell. Other cation and anion positions are deleted for clarity.

According our new x-ray diffraction studies, the monoclinic lattice parameters of PYN are found to be $a_m = b_m = 4.168$ Å, $c_m = 4.110$ Å and $\gamma_m = 89.47^\circ$ at room temperature and the orthorhombic lattice parameters are found to be:

$$\begin{aligned} a_o &= |\boldsymbol{b}_m - \boldsymbol{a}_m| = 2a_m \sin(\gamma_m/2) = 5.866 \text{ Å} \\ b_o &= 4|\boldsymbol{a}_m + \boldsymbol{b}_m| = 8a_m \cos(\gamma_m/2) = 23.684 \text{ Å} \\ c_o &= 2|\boldsymbol{c}_m| = 8.219 \text{ Å}. \end{aligned} \tag{3}$$

Consequently, a_o becomes slightly smaller than $b_o/4$ (=5.921 Å) due to the contraction of the monoclinic cell along the $\boldsymbol{a}_o$ direction.

3.2. Point group

Until now, scanty results regarding the crystal structure of antiferroelectric PYN have been published. But no systematic investigation of the positions of Yb, Nb and O atoms has been performed. It is very important to find the symmetry elements related to all atoms of PYN. Even in the case of $PbZrO_3$, there have been disagreements on whether the lead and oxygen atoms occupy centrosymmetric positions or not [14, 15]. There are three point groups in orthorhombic system. They are 222, $mm2$ and mmm. In order to become typically antiferroelectric, the point group of PYN ought to be mmm. To analyse the domain-wall orientation of PYN, it is absolutely necessary to know its exact point group.

Figure 4 shows three different CBED patterns: (a) the full WP (whole pattern), (b) the projection WP and (c) the BF (bright field) pattern from the (0 0 0) spot of PYN. The beam incidence is in the direction of $[0\,8\,0]_o$ $(=[1\,1\,0]_m)$. The symmetries of the full and projection diffraction in WP and BF patterns are all $2mm$. In the full patterns of (a) WP and (c) BF, two mirror planes perpendicular to the $\boldsymbol{a}_o^*$ and $\boldsymbol{c}_o^*$ axes are observed and intersect at

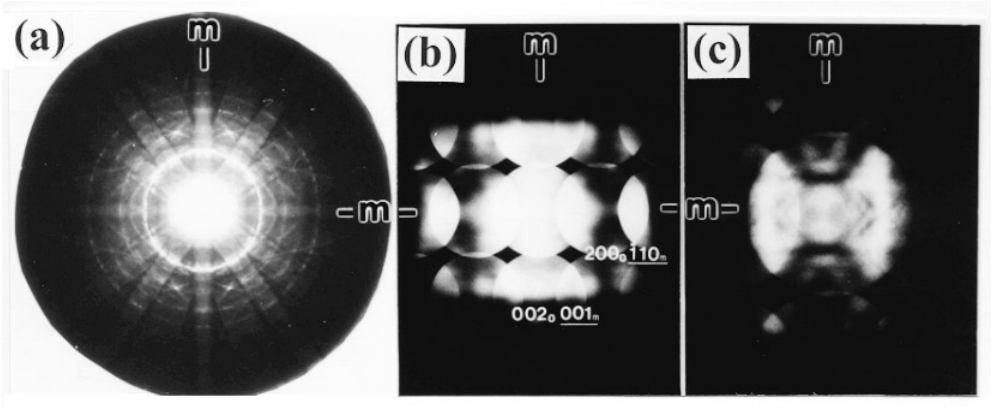

Figure 4. $[0\,8\,0]_o$ $(=[1\,1\,0]_m)$ zone-axis patterns from antiferroelectric $Pb(Yb_{1/2}Nb_{1/2})O_3$: (a) the full WP, (b) the projection WP and (c) the BF disc. All the patterns possess $2mm$ symmetry.

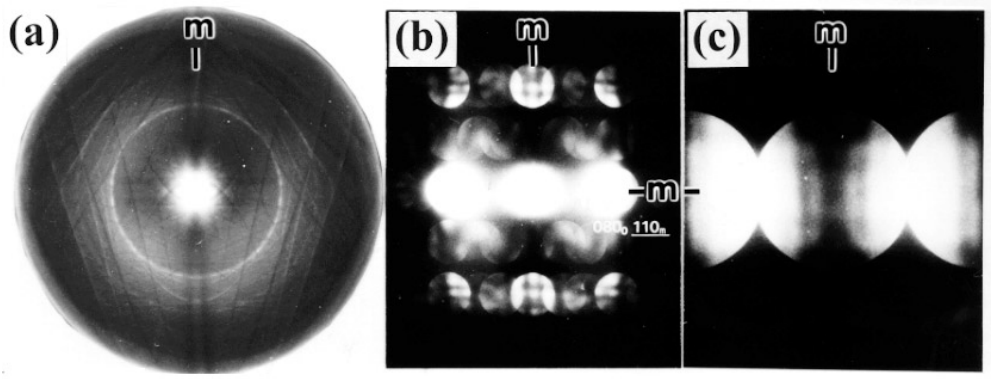

Figure 5. $[2\,0\,4]_o$ $(=[\bar{1}\,1\,2]_m)$ zone-axis patterns from antiferroelectric $Pb(Yb_{1/2}Nb_{1/2})O_3$: (a) the full WP, (b) the BF and (c) the WP of projection symmetry.

the zone axis. Figure 5 represents CBED patterns taken with the $[2\,0\,4]_o$ $(=[\bar{1}\,1\,2]_m)$ beam incidence. It has a full WP of reflection symmetry as shown in figure 5(a). But figures 5(b) and (c) show that the projection symmetries of BF and WP are $2mm$. In the full WP pattern, there is one mirror plane which is perpendicular to the $\boldsymbol{b}_o^*$ axis. It is certain that there exist mirror planes perpendicular to the three mutually orthogonal directions of the orthorhombic lattice.

With reference to the tables of Buxton *et al* [16], the symmetries of CBED patterns can be predicted from each point group. Table 1 represents the relationship between the symmetries of CBED patterns and the point groups of the three orthorhombic systems for the observed zones. It can be found that the symmetries observed from the two zones are in accord with those of the point group mmm. Further, other zone axes also showed symmetries expected from the mmm point group by the Buxton's tables. Thus with reference to table 1, the point group of antiferroelectric PYN can unequivocally be established as mmm.

It is now firmly established from the CBED results that there are only three mirror planes corresponding to the mutually orthogonal $(1\,1\,0)_m$, $(1\,\bar{1}\,0)_m$ and $(0\,0\,1)_m$ planes in

Table 1. Diffraction groups and symmetries of CBED patterns expected from the three orthorhombic systems for $[080]_o$ and $[204]_o$ incidences [16].

			Full symmetry		Projection symmetry	
Zone	Point group	Diffraction group	WP	BF	WP	BF
$[080]_o$	mmm	$2mm1_R$	$2mm$	$2mm$	$2mm$	$2mm$
	$mm2$	$m1_R$	$2mm$	m	$2mm$	m
	222	$2m_Rm_R$	$2mm$	2	$2mm$	$2mm$
$[204]_o$	mmm	2_Rmm_R	m	m	$2mm$	$2mm$
	$mm2$	m	m	m	$2mm$	m
	222	m_R	m	1	$2mm$	m

antiferroelectric PYN. It is predicted from the group theoretical approach that the $(1\,0\,0)_m$, $(0\,1\,0)_m$, $(0\,1\,1)_m$, $(0\,\bar{1}\,1)_m$, $(\bar{1}\,0\,1)_m$ and $(1\,0\,1)_m$ domain walls reestablish the reflection symmetries broken on transition from the prototype to low-symmetry phase and form W-walls in ferroelastic phase.

3.3. Domain-wall orientations

According to Aizu [17], a crystal is said to be ferroelastic if it can possess two or more equally stable orientational states in the absence of mechanical stress or electric field. The orientation state can be switched from one to another by the application of a temporary mechanical stress. The ferroelastic crystals are characterized by the spontaneous strain tensor e^s that represents a small deformation in the ferroelastic phase with respect to the paraelastic phase [18]. From the spontaneous strain compatibility defined by Fousek and Janovec [9] for ferroelectric crystals, Sapriel theoretically predicted the orientations of domain walls in all the ferroelastic crystals [8]. He used a criterion that the permissible walls should be strain free, i.e. that along all directions in the wall the strains should be same for the two orientational states.

As previously stated, PYN undergoes a ferroelastic transition as well as an antiferroelectric one from the prototype in the vicinity of 300 °C. From the results of the aforementioned CBED analysis, the transition is shown to change the point group of PYN from the high-temperature cubic $m3m$ to low-temperature orthorhombic mmm. The Aizu species of PYN are thus classified as $m3mFmmm$ [17]. It is found that the symmetry elements lost at the PYN transition are reflections and twofold rotations as illustrated in figure 6. Let a particular ferroelastic domain D_1 with the orthorhombic lattice be chosen as a reference. The point group of D_1 with respect to the prototype phase coordinate system is $F = m_{xy}\bar{m}_{xy}m_z$. According to group analysis [7], the point group G of the prototypic phase can be expressed by the decomposition of $m3m$ into left cosets of the subgroub mmm:

$$G = m3m = F + m_xF + 2_{yz}F + \bar{2}_{yz}F + \bar{2}_{xz}F + 2_{xz}F. \tag{4}$$

Accordingly, all the other domains can be generated from domain D_1 by applying to D_1 the symmetry operations of the point group G which do not belong to F. We can find that there are six different orientational states, i.e. domains D_1–D_6 in PYN.

Let us examine the relation between the spontaneous strain and the orientations of domain walls. The strain tensor of the orientation state D_1 in reference to the

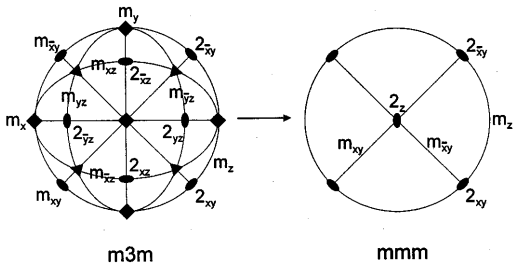

Figure 6. Stereogram of the symmetry changes in the $Pb(Yb_{1/2}Nb_{1/2})O_3$ crystal.

undistorted/rotated orthorhombic lattice frame is given as

$$e_o(\mathrm{D}_1) = \begin{bmatrix} e_{11} & 0 & 0 \\ & e_{22} & 0 \\ & & e_{33} \end{bmatrix}_o \tag{5}$$

where

$$\begin{aligned} (e_{11})_o &= \frac{a_o - a_c'\sqrt{2}}{a_c'\sqrt{2}} \\ (e_{22})_o &= \frac{b_o/4 - a_c'\sqrt{2}}{a_c'\sqrt{2}} \\ (e_{33})_o &= \frac{c_o/\sqrt{2} - a_c'\sqrt{2}}{a_c'\sqrt{2}}. \end{aligned} \tag{6}$$

The strain matrix, equation (5), is not traceless. To make it traceless, we need to subtract an averaged diagonal matrix $\bar{e}_o(\mathrm{D})$ from $e_o(\mathrm{D}_1)$,

$$e_o^s(\mathrm{D}_1) = e_o(\mathrm{D}_1) - \bar{e}_o(\mathrm{D}) \tag{7}$$

where

$$\bar{e}_o(\mathrm{D}) = \frac{1}{6}\sum_{j=1}^{6} e_o(\mathrm{D}_j) = \frac{1}{3} = \begin{bmatrix} e_{11}+e_{22}+e_{33} & 0 & 0 \\ & e_{11}+e_{22}+e_{33} & 0 \\ & & e_{11}+e_{22}+e_{33} \end{bmatrix}_o. \tag{8}$$

The $e_o^s(\mathrm{D}_1)$ of equation (7) is indeed the Aizu spontaneous strain and is now

$$e_o^s(\mathrm{D}_1) = \begin{bmatrix} \frac{(2e_{11}-e_{22}-e_{33})}{3} & 0 & 0 \\ & \frac{(-e_{11}+2e_{22}-e_{33})}{3} & 0 \\ & & \frac{(-e_{11}-e_{22}+2e_{33})}{3} \end{bmatrix}_o. \tag{9}$$

From the high-temperature x-ray diffraction method, we could obtain the variations of the strain components with temperature as shown in figure 7. The value of a_c' was obtained by extrapolating the lattice parameter a_c measured in the prototype at the desired temperature and estimated to be 4.156 Å at room temperature. At room temperature, the values of orthorhombic strains $(e_{11})_o$, $(e_{22})_o$ and $(e_{33})_o$ were evaluated to be -1.884×10^{-3}, 7.406×10^{-3} and -11.139×10^{-3}, respectively.

Actually the undistorted orthorhombic lattice frame is rotated by 45° about the $\boldsymbol{c}_o$ ($\boldsymbol{c}_c$) axis from the prototype cubic lattice frame. Both the Sapriel and Aizu strains are formulated with respect to the prototype lattice reference frame. The corresponding strains in reference

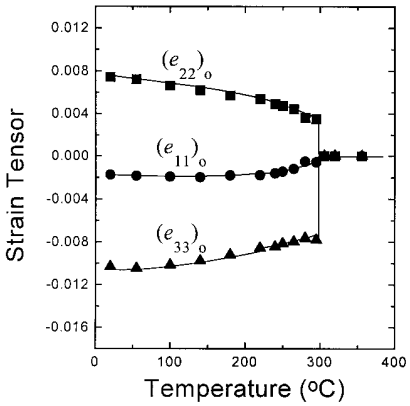

Figure 7. Temperature dependence of the orthorhombic strain components, $(e_{11})_o$, $(e_{22})_o$ and $(e_{33})_o$.

to the prototype crystal system can be readily obtained by operating similarity transformation $\mathbf{T}^{-1}e_o^s(\mathrm{D}_1)\mathbf{T}$ on $e^s(\mathrm{D}_1)$. The coordinate transformation matrix $\mathbf{T}(\mathrm{D}_1)$ is

$$\mathbf{T}(\mathrm{D}_1) = \begin{bmatrix} \frac{1}{\sqrt{2}} & \frac{1}{\sqrt{2}} & 0 \\ -\frac{1}{\sqrt{2}} & \frac{1}{\sqrt{2}} & 0 \\ 0 & 0 & 1 \end{bmatrix}. \tag{10}$$

Herein we can also consider each column of $\mathbf{T}$ as a unit basis vector respectively of the orthorhombic axes with respect to the cubic prototype lattice frame. The resultant Aizu strain $e^s(\mathrm{D}_1)$ obtained in the Sapriel notation is

$$e^s(\mathrm{D}_1) = \begin{bmatrix} b & d & 0 \\ & b & 0 \\ & & -2b \end{bmatrix} \tag{11}$$

where

$$b = \frac{(e_{11})_o + (e_{22})_o - 2(e_{33})_o}{6} \qquad \text{and} \qquad d = \frac{(e_{11})_o - (e_{22})_o}{2}. \tag{12}$$

On transition from high-temperature prototype phase to low-temperature orthorhombic phase, the monoclinic spontaneous strains relative to the cubic prototype lattice are created. Hence, the low-temperature crystal may be looked upon as a monoclinically distorted phase with a lattice modulation in the $\boldsymbol{b}_o(=(1/\sqrt{2})[110]_c)$ direction.

It is straightforward to derive the coordinate transformation matrix $\mathbf{T}(\mathrm{D}_j)$ corresponding to the orientation state D_j obtained by symmetry operation of the left coset elements given in equation (4). Hence we will only give the rest of the strain matrices obtained by similarity transformation $\mathbf{T}^{-1}(\mathrm{D}_j)e^s(\mathrm{D}_1)\mathbf{T}(\mathrm{D}_j)$ in the following:

$$\text{on } m_x \text{ operation, } e^s(\mathrm{D}_2) = \begin{bmatrix} b & -d & 0 \\ & b & 0 \\ & & -2b \end{bmatrix}$$

$$\text{on } 2_{yz} \text{ operation, } e^s(\mathrm{D}_3) = \begin{bmatrix} b & 0 & -d \\ & -2b & 0 \\ & & b \end{bmatrix}$$

$$\text{on } 2^-_{yz} \text{ operation, } e^s(\mathrm{D}_4) = \begin{bmatrix} b & 0 & d \\ & -2b & 0 \\ & & b \end{bmatrix} \tag{13}$$

$$\text{on } 2^{-}_{xz} \text{ operation, } e^s(\mathrm{D}_5) = \begin{bmatrix} -2b & 0 & 0 \\ & b & d \\ & & b \end{bmatrix}$$

$$\text{on } 2_{xz} \text{ operation, } e^s(\mathrm{D}_6) = \begin{bmatrix} 2b & 0 & 0 \\ & b & -d \\ & & b \end{bmatrix}.$$

The possible orientations of domain walls between any two adjacent domains, D_i and D_j ($i \neq j$), can be derived from the equations of the strain-compatibility condition [8]

$$\{e^s(\mathrm{D}_j) - e^s(\mathrm{D}_i)\}x_k x_l = 0 \qquad (k, l = 1, 2, 3) \tag{14}$$

where x_k and x_l are the components of a vector contained in the wall.

Table 2 shows the equations of permissible domain-wall orientations in low-temperature phase PYN. In the second column of table 2, the plane equations of the permissible domain walls are given. Twenty-one independent equations out of a possible 30 were given by Sapriel in the $m3mFmmm$ transition with the strain matrix in the form of equation (11). If our plane equations look different from Sapriel's at a first glance, it is because we chose the $\boldsymbol{c}_c$ ($\boldsymbol{c}_m$) axis as the unique axis whereas Sapriel chose the $\boldsymbol{a}_c$ ($\boldsymbol{c}_m$) axis as the unique one. Both sets of equations are equivalent if the crystal axes are properly exchanged. In addition to the plane equations in Sapriel's table, we give more information on the adjoining domain pairs $\mathrm{D}_i\mathrm{D}_j$ separated by a domain wall in the first column. In the third column, we paraphrase the high-symmetry planes with the Miller indices in reference to the distorted monoclinic lattice frame. Also note that the left plane on each row of columns 2 and 3 is normal to the right plane. It is often the case that a high-symmetry domain W-wall is normal to a low-symmetry W′-wall as was designated by Sapriel. The W′-walls are in fact mediated by strain since their orientations are constrained by the strain elements b and d whereas the high-symmetry W-walls are not.

Table 2. Possible walls in $Pb(Yb_{1/2}Nb_{1/2})O_3$.

Domain pairs $\mathrm{D}_i\mathrm{D}_j$	Permissible walls		Monoclinic indexing of the wall with respect to each domain				Type of W-wall
			D_i		D_j		
$\mathrm{D}_1\mathrm{D}_2$	$x = 0$	$y = 0$	(1 0 0)	(0 1 0)	$(\bar{1}\,0\,0)$	(0 1 0)	90°
$\mathrm{D}_1\mathrm{D}_3$	$y = -z$	$3b(z-y) - 2dx = 0$	(0 1 1)	—	(0 1 1)	—	120°
$\mathrm{D}_1\mathrm{D}_4$	$y = z$	$3b(z+y) + 2dx = 0$	$(0\,1\,\bar{1})$	—	$(0\,1\,\bar{1})$	—	120°
$\mathrm{D}_1\mathrm{D}_5$	$z = x$	$3b(z+x) + 2dy = 0$	$(\bar{1}\,0\,1)$	—	$(\bar{1}\,0\,1)$	—	120°
$\mathrm{D}_1\mathrm{D}_6$	$z = -x$	$3b(z-x) - 2dy = 0$	(1 0 1)	—	(1 0 1)	—	120°
$\mathrm{D}_2\mathrm{D}_3$	$y = z$	$3b(z+y) - 2dx = 0$	$(0\,1\,\bar{1})$	—	$(0\,\bar{1}\,1)$	—	60°
$\mathrm{D}_2\mathrm{D}_4$	$y = -z$	$3b(z-y) + 2dx = 0$	(0 1 1)	—	$(0\,\bar{1}\,\bar{1})$	—	60°
$\mathrm{D}_2\mathrm{D}_5$	$z = -x$	$3b(z-x) + 2dy = 0$	$(\bar{1}\,0\,1)$	—	$(\bar{1}\,0\,\bar{1})$	—	120°
$\mathrm{D}_2\mathrm{D}_6$	$z = x$	$3b(z+x) - 2dy = 0$	(1 0 1)	—	$(1\,0\,\bar{1})$	—	120°
$\mathrm{D}_3\mathrm{D}_4$	$z = 0$	$x = 0$	(0 1 0)	$(\bar{1}\,0\,0)$	$(0\,\bar{1}\,0)$	$(\bar{1}\,0\,0)$	90°
$\mathrm{D}_3\mathrm{D}_5$	$x = -y$	$3b(y-x) + 2dz = 0$	$(\bar{1}\,0\,1)$	—	$(0\,\bar{1}\,\bar{1})$	—	120°
$\mathrm{D}_3\mathrm{D}_6$	$x = y$	$3b(x+y) - 2dz = 0$	$(\bar{1}\,0\,\bar{1})$	—	(0 1 1)	—	60°
$\mathrm{D}_4\mathrm{D}_5$	$x = y$	$3b(x+y) + 2dz = 0$	$(\bar{1}\,0\,1)$	—	$(0\,1\,\bar{1})$	—	60°
$\mathrm{D}_4\mathrm{D}_6$	$x = -y$	$3b(y-x) - 2dz = 0$	$(\bar{1}\,0\,\bar{1})$	—	$(0\,\bar{1}\,1)$	—	120°
$\mathrm{D}_5\mathrm{D}_6$	$y = 0$	$z = 0$	$(0\,\bar{1}\,0)$	$(\bar{1}\,0\,0)$	$(0\,\bar{1}\,0)$	(1 0 0)	90°

Sapriel gave further insight into the nature of W-walls and W′-walls. The W-walls are entirely determined by symmetry alone and are parallel to prominent mirror planes of

the prototype phase which disappear during ferroelastic transition. A W′-wall is parallel to a prototype twofold axis which loses its presence in the ferroelastic state. The latter is not determined by symmetry alone since one angular degree of freedom remains. In the stereogram, figure 6, which depicts the symmetry change during PYN transition, we can clearly see the restoration of mirror planes m_x, m_y, m_{yz}, m^-_{yz}, m^-_{xz} and m_{xz} on domain formation which disappear in the ferroelastic phase. In the meantime, the disappearing twofold axes, 2_{yz} $(=[0\,1\,1]_c)$, 2^-_{yz} $(=[0\,\bar{1}\,1]_c)$, 2^-_{xz} $(=[\bar{1}\,0\,1]_c)$ and 2_{xz} $(=[1\,0\,1]_c)$, during transition can be retained on W′-wall formation in Sapriel's terminology. The plane equations in table 2 which contain b and d represent the W′-walls. As a W′-wall contains one of the above four twofold axes, its orientation is determined under the constraint that the interface is strain free.

A W-wall is oriented parallel to a crystallographically prominent plane of fixed indices. Its orientation does not change with temperature. In table 2 the W-walls in PYN are initially identified as the two-fold degenerate $\{1\,0\,0\}_c$ and six-fold degenerate $\{1\,1\,0\}_c$ planes. These planes are indexed in reference to the pseudo-cubic lattice. In the monoclinic lattice frame, we find that the number of these planes are reduced to six walls, $(1\,0\,0)_m$, $(0\,1\,0)_m$, $(0\,1\,1)_m$, $(0\,\bar{1}\,1)_m$, $(\bar{1}\,0\,1)_m$ and $(1\,0\,1)_m$ as described in the third column of table 2. These planes correspond to the mirror planes lost on transition, i.e. m_x, m_y, m_{yz}, m^-_{yz}, m^-_{xz} and m_{xz}, respectively. The lattice of orthorhombic PYN is additionally modulated due to antiparallel displacements of Pb^{2+} ions along the $\boldsymbol{a}_o$ $(=[1\,\bar{1}\,0]_m)$ direction. With respect to the modulation vector (parallel to $\boldsymbol{b}_o = [1\,1\,0]_m$), the domain wall cannot be produced in any arbitrary fashion, but there are only three possible ways to form the W-walls. Figure 8 shows such walls of twinlike boundary structure separating the adjacent domains, which are described in the monoclinic lattice frame ($a_m \times b_m \times c_m \approx a'_c \times a'_c \times a'c$).

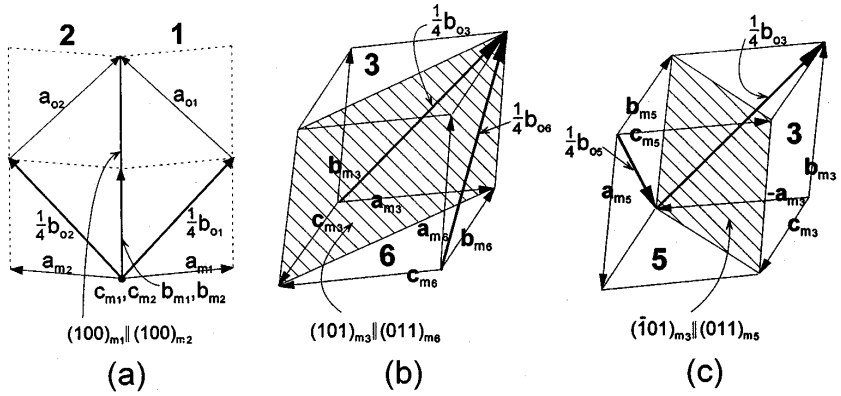

Figure 8. Possible twin lattice structures in $Pb(Yb_{1/2}Nb_{1/2})O_3$: (a) 90°, (b) 60° and (c) 120° domain boundaries.

The ferroelectric domain-boundaries are classified according to whether they are 90° or 180° domain boundaries by the angle between the polarizations of the two bordering domains. In analogy to the ferroelectric case, we devised a scheme for classifying the ferroelastic PYN domain walls whether they are 60°, 90° or 120° walls. The angle between the two bordering domains was defined as the angle at which the two modulation wavevectors of the two domains meet. The $\boldsymbol{b}_o$ vectors, which are parallel to the modulation wavevectors of the D_1, D_2, D_3, D_4, D_5 and D_6 domains are respectively along $[1\,1\,0]_c$, $[\bar{1}\,1\,0]_c$, $[\bar{1}\,0\,1]_c$, $[\bar{1}\,0\,\bar{1}]_c$, $[0\,\bar{1}\,\bar{1}]_c$ and $[0\,\bar{1}\,1]_c$. The permissible walls between D_1 and D_2

are either $(1\,0\,0)_m$ and $(0\,1\,0)_m$, and the angle between the D_1 and D_2 modulation directions is nearly 90°. Hence the $(1\,0\,0)_m$ and $(0\,1\,0)_m$ domain walls may be defined as 90° walls according to the scheme described above. The near 90° angle between the modulation vectors of D_1 and D_2 domains is sketched in figure 8(a). In a similar manner, the D_3D_4 and D_5D_6 domain pairs also form 90° domain boundaries.

Figure 8(b) shows how a 60° domain may be formed. The $\boldsymbol{b}_o$ vectors respectively of D_3 and D_6 domains meet at a 60° angle. Hence the domain wall separating D_3 and D_6 domains may be defined as a 60° domain wall. Figure 8(c) shows that the domain wall between D_3 and D_5 domains is a 120° domain wall. All the possible types of PYN W-wall are illustrated in the fourth column of table 2. We notice in the table that either $(1\,0\,0)_m$ or $(0\,1\,0)_m$ forms a 90° W-wall, while the $(0\,1\,1)m$, $(0\,\bar{1}\,1)m$, $(\bar{1}\,0\,1)_m$ and $(1\,0\,1)_m$ walls form 60° or 120° W-walls.

The orientations of W′-walls, represented by irrational indices which may only accidentally become rational, can be determined by the b and d components of the spontaneous strain tensor, and thus should vary with temperature. For PYN, a W′-wall always contains one of the twofold axes, 2_{yz} $(=[0\,1\,1]_c)$, 2^{-}_{yz} $(=[0\,\bar{1}\,1]_c)$, 2^{-}_{xz} $(=[\bar{1}\,0\,1]_c)$ and $2_{xz}(=[1\,0\,1]_c)$, and can change its orientation as temperature is changed. From the tensor components of figure 7 and equation (12), we can determine the temperature dependence of b and d as shown in figure 9. At room temperature b and d have nearly the same magnitude but are opposite in sign ($b = 4.633 \times 10^{-3}$ and $d = -4.645 \times 10^{-3}$). This indicates that from the equations of the permissible domain walls in table 2, the W′-wall planes are approximately $(\bar{2}\,3\,3)_m$, $(2\,\bar{3}\,3)_m$, $(\bar{3}\,2\,3)_m$ and $(3\,\bar{2}\,3)_m$ at room temperature. The b/d ratio shows little change with temperature up to about 220 °C. However, approaching the transition temperature from below, the magnitude of the ratio increases fast. This means that in the vicinity of T_C the orientation of W′-walls changes rapidly on account of large variation of the lattice distortion. At 280 °C b/d is about -1.5 and the W′-walls become almost $(\bar{4}\,9\,9)_m$, $(4\,\bar{9}\,9)_m$, $(\bar{9}\,4\,9)_m$ and $(9\,\bar{4}\,9)_m$ planes. As the temperature increases further, the magnitude of the ratio should increase more. As the trend toward increasing the magnitude of the ratio continues, the orientations of W′-walls would look more like those of 60° or 120° W-walls. Only the first-order character of PYN phase transition can prevent the W′-walls ever becoming 60° or 120° W-walls near the transition. We guess that the PYN W′-walls reorient themselves toward the W-wall orientation with increasing temperature.

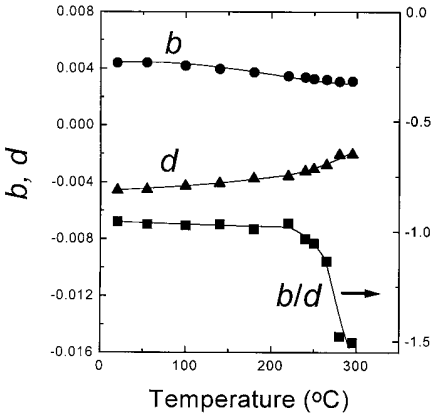

Figure 9. Variation of Sapriel's strain elements b, d and the b/d ratio with temperature.

4. Conclusions

We have looked into the crystal structure again and the domain wall orientations of ferroelastic/antiferroelectric $Pb(Yb_{1/2}Nb_{1/2})O_3$ by TEM. PYN is orthorhombic and its point group is determined to be *mmm* by CBED studies. The prototype cubic cell experiences monoclinic distortion during transition from the cubic to the orthorhombic. Below T_C, the monoclinic cell dimension is slightly contracted along the direction of Pb^{2+} shifts.

The mirror planes (1 0 0), (0 1 0), (0 1 1), (0 $\bar{1}$ 1), ($\bar{1}$ 0 1) and (1 0 1) of PYN disappear on transition from the cubic to orthorhombic phase. These planes can reappear as W-walls in the ferroelastic phase. From the geometrical consideration, the $(1\,0\,0)_m$ and $(0\,1\,0)_m$ planes become 90° domain boundaries and the rest become both 60° and 120° ones. The non-prominent domain-boundaries, W′-walls were calculated by making use of *b* and *d* values derived from the equation of the strain-compatibility condition. The W′-wall planes are approximately $(\bar{2}\,3\,3)_m$, $(2\,\bar{3}\,3)_m$, $(\bar{3}\,2\,3)_m$ and $(3\,\bar{2}\,3)_m$ at room temperature. On approaching the transition these W′-walls are seen to move toward the orientation of 60° or 120° domain boundaries.

Acknowledgment

The authors appreciate the financial support from the Research Centre for Dielectric and Advanced Matter Physics (RCDAMP) at Pusan National University for this work.

References

[1] Tomashpol'skii Y Y and Venevtsev Y N 1965 *Sov. Phys.–Solid State* **6** 2388
[2] Smolenskii G A, Agranovskaya A I, Popov S N and Isupov V A 1959 *Sov. Tech. Phys.* **3** 1981
[3] Isupov V A and Krainik N N 1965 *Sov. Phys.–Solid State* **6** 2975
[4] Kwon J R and Choo W K 1991 *J. Phys.: Condens. Matter* **3** 2147
[5] Sawaguchi E, Maniwa H and Hoshino S 1951 *Phys. Rev.* **83** 1078
[6] Kwon J R, Choo C K K and Choo W K 1991 *Japan. J. Appl. Phys.* **30** 1028
[7] Janovec V 1972 *Czech. J. Phys.* B **22** 974
[8] Sapriel J 1975 *Phys. Rev.* B **12** 5128
[9] Fousek J and Janovec V 1969 *J. Appl. Phys.* **40** 135
[10] Swartz S L and Shrout T R 1982 *Mater. Res. Bull.* **17** 1245
[11] Shatalova G E, Filiper V S, Katsnel'son L M and Fesenko E G 1974 *Sov. Phys.–Crystallogr.* **19** 257
[12] Fujishita H, Shiozaki Y and Sawaguchi E 1979 *J. Phys. Soc. Japan* **46** 1391
[13] Whatmore R W and Glazer A M 1979 *J. Phys. C: Solid State Phys.* **12** 1505
[14] Jona F, Shirane G, Mazzi F and Pepinsky R 1957 *Phys. Rev.* **105** 849
[15] Fujishita H and Hashino S 1984 *J. Phys. Soc. Japan* **53** 226
[16] Buxton B F, Eades J A, Steeds J W and Rackham G M 1976 *Phil. Trans. R. Soc.* A **281** 171
[17] Aizu K 1969 *J. Phys. Soc. Japan* **27** 387
[18] Aizu K 1970 *J. Phys. Soc. Japan* **28** 706